

Phase diagram of $S = 1$ XXZ chain with next-nearest-neighbor interactionTAKAHIRO MURASHIMA¹, KEIGO HIJII¹, KIYOHIDE NOMURA¹ and TAKASHI TONEGAWA²¹*Department of Physics, Kyushu University, Fukuoka 812-8581, Japan*²*Department of Mechanical Engineering, Fukui University of Technology, Fukui 910-8505, Japan*

The one dimensional $S = 1$ XXZ model with next-nearest-neighbor interaction α and Ising-type anisotropy Δ is studied by using a numerical diagonalization technique. We discuss the ground state phase diagram of this model numerically by the twisted-boundary-condition level spectroscopy method and the phenomenological renormalization group method, and analytically by the spin wave theory. We determine the phase boundaries among the XY phase, the Haldane phase, the ferromagnetic phase and the Néel phase, and then we confirm the universality class. Moreover, we map this model onto the non-linear σ model and analyze the phase diagram in the $\alpha \ll -1$ and $\Delta \sim 1$ region by using the renormalization group method.

KEYWORDS: spin-1, ground state phase diagram, frustration, diagonalization, level spectroscopy, non-linear σ model

1. Introduction

One dimensional antiferromagnetic Heisenberg spin systems have been an important subject in many-body physics for a long time. There are no ordered ground states with a continuous symmetry breaking in these systems, because of quantum fluctuation and low dimensionality. It is well known from Haldane's conjecture^{1,2} that there is a fundamental difference between half-integer and integer spin chains in their low-lying excitations. In some lattice systems, frustration, which is geometrically represented by a triangular lattice, tends to disorder the ground state. We expect that competing systems between quantum fluctuation and frustration plus low dimensionality exhibit fascinating phenomena in their ground states and low-lying excitations. Recently, the materials of the $S = 1$ spin chain with next-nearest-neighbor interaction have been reported experimentally (CaV_2O_4 ,³ $\text{NaV}(\text{WO}_4)_2$ ⁴).

In this paper, we study the $S = 1$ XXZ chain with next-nearest-neighbor (NNN) interaction, which is described by the following Hamiltonian:

$$\begin{aligned} \mathcal{H} = & \sum_{i=1}^L (S_i^x S_{i+1}^x + S_i^y S_{i+1}^y + \Delta S_i^z S_{i+1}^z) \\ & + \alpha \sum_{i=1}^L (S_i^x S_{i+2}^x + S_i^y S_{i+2}^y + \Delta S_i^z S_{i+2}^z), \end{aligned} \quad (1)$$

where α is next-nearest-neighbor interaction constant and L is system size (L : even). Hereafter, periodic boundary condition (PBC) will be assumed unless specifically mentioned.

A phase diagram of this model has been studied by the exact diagonalization method for the $|\Delta| < 2$ and $0 \leq \alpha < 0.3$ region,⁵ and also by the infinite-system density matrix renormalization group method (DMRG) for the $\Delta \geq 0$ and $\alpha \geq 0$ region.^{6,7} Many phases of the ground state have been found there; the Haldane phase, the double Haldane phase, the Néel phase, the double Néel phase, the gapped chiral phase and the gapless chiral phase. The features of these phases are explained simply as follows. The Haldane state has an energy gap, where the spin correlation decreases exponentially as $L \rightarrow \infty$. The Néel state is characterized by twofold degenerate ground states, where the staggered magnetization exhibits a long range order. In the double Haldane phase, the system can be regarded as two Haldane subchains because of competition between the strong next-nearest-neighbor interaction and the weak nearest-neighbor interaction. A first-order phase transition occurs between the Haldane phase and the double Haldane phase.^{8,9} We can also regard the double Néel state as two Néel subchains (up-down-up-down or up-up-down-down). The gapped chiral state and the gapless chiral state have a chiral long range order, whereas the two spin correlation decays exponentially in the former state and algebraically in the latter one.^{6,7}

On the $\alpha = 0$ line, it is known that four different ground states exist; the ferromagnetic state ($\Delta \leq -1$), the XY state ($-1 \leq \Delta \leq 0$), the Haldane state ($0 \leq \Delta \lesssim 1.17$) and the Néel state ($1.17 \gtrsim \Delta$).¹⁰⁻¹³ The ferromagnetic state has a long range order of the magnetization. In the XY phase, the spin correlation shows an algebraic decay, and the correlation length is infinite. A first-order phase transition occurs between the ferromagnetic phase and the XY phase, and the 2D-Ising type phase transition occurs between the Haldane phase and the Néel phase.¹³

It has been well known that the Berezinskii-Kosterlitz-Thouless (BKT) transition occurs between the XY phase and the Haldane phase, which is explained by the bosonization method for a spin- s XXZ model.¹⁴ This transition belongs to the infinite-order phase transition in the traditional classification. On this transition point, the logarithmic correction appears in the correlation function, the critical exponents and so on. Numerically, the BKT transition has been known to occur at the $\Delta = 0$ and $\alpha = 0$ point in a spin-1 ($S = 1$) XXZ model with bond alternation constant δ for $|\delta| < 0.23$,^{10,11} and that with uniaxial single-ion-type anisotropy constant D for $-2 < D < 0.5$.¹² A bosonization study for a spin- s XY model with NNN interaction has supported that this particular point is determined as the BKT transition point in the $S = 1$ case.¹⁵ Recently, the fact that this point ($\Delta = \alpha = 0$) is the BKT transition point has been analytically proved.¹⁶ For many years, it was a difficult problem to determine numerically the critical point and the universality class of the BKT transition, because of logarithmic corrections and the slow divergence of the correlation length. Although the DMRG method is a powerful method to examine many phases, it is not appropriate to determine the BKT transition line. This problem was successfully resolved by the level

spectroscopy method,¹⁷ based on the conformal field theory and the renormalization group. Moreover, this method was improved by the twisted-boundary-condition level spectroscopy method.¹⁸ We use the twisted-boundary-condition level spectroscopy method to determine the BKT transition point when $\Delta \neq 0$ or $\alpha \neq 0$.

In this work, we present a phase diagram of the $S = 1$ XXZ chain with NNN interaction, analyzing the diagonalization data by the twisted-boundary-condition level spectroscopy method,¹⁸ the phenomenological renormalization group (PRG) method,^{19,20} the spin wave theory and the renormalization group method.

This paper is organized as follows. In the next section, the obtained phase diagram is presented. The numerical methods to determine the phase boundaries are explained in §3. In §4, we map eq. (1) onto the non-linear σ model, and then we analytically examine the phase diagram in the region of $\alpha \ll -1$ and $\Delta \sim 1$. The final section is devoted to a summary and a discussion.

2. Phase diagram

The obtained phase diagram is summarized in Fig. 1, which consists of the ferromagnetic phase, the XY phase, the Haldane phase and the Néel phase. We have determined the BKT transition line between the XY and Haldane phases by using the twisted-boundary-condition level spectroscopy method.¹⁸ Then, from the analysis of the spin wave theory, we determine the first-order phase transition line between the ferromagnetic and XY phases, and that between the ferromagnetic and Haldane phases. Moreover, the Haldane-Néel transition line is determined by the PRG method.^{19,20}

In the $\alpha > 0.4$ region, it is expected that the gapped and gapless chiral phases, the double Haldane phase and the double Néel phase appear in the phase diagram.⁶⁻⁹ Since the level spectroscopy and PRG methods do not work in this region because of incommensurability, we do not treat this region in this study. This point will be discussed further in §5.

3. Numerical methods and results

3.1 Level spectroscopy and BKT transition

In this subsection, we briefly review the level spectroscopy method¹⁷ and the twisted-boundary-condition level spectroscopy method,¹⁸ and then we determine the BKT transition line using the latter method. In addition, we check the consistency of the universality class.

With the use of the bosonization technique,¹⁴ the one dimensional XXZ spin system can be mapped onto the following sine-Gordon model (in Euclidean space-time):

$$S = \frac{1}{2\pi K} \int d\tau dx \{ (\partial_\tau \phi)^2 + (\partial_x \phi)^2 \} + \frac{y_2}{2\pi a^2} \int d\tau dx \cos \sqrt{2}\phi, \quad (2)$$

where $\phi \equiv \phi(\tau, x)$ is the boson field and a is the lattice constant. After a scaling transformation

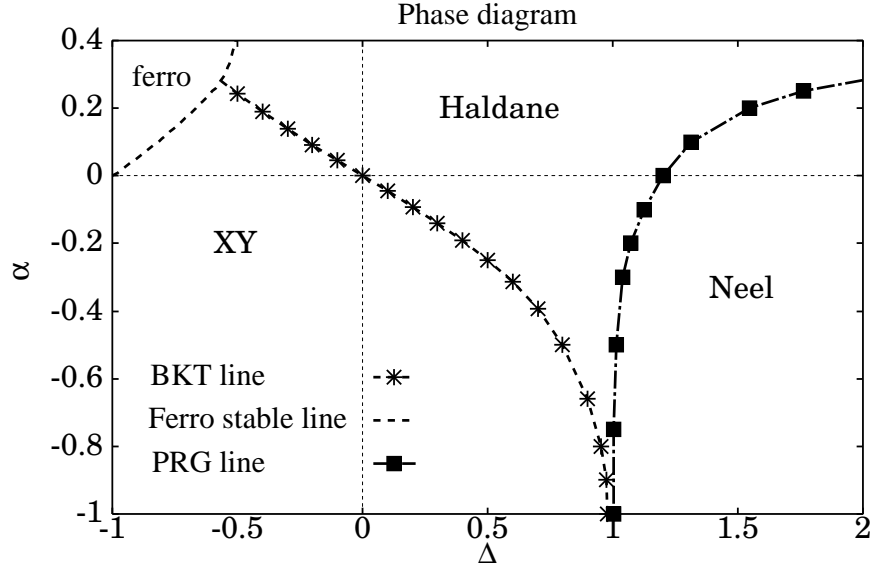


Fig. 1. Phase diagram of the $S = 1$ XXZ chain with next-nearest-neighbor interaction in the region of $-1 \leq \Delta \leq 2$ and $-1 \leq \alpha \leq 0.4$. Note that the ferromagnetic stable line for $\alpha > 0.4$ is given in Fig. 6.

$a \rightarrow e^{\delta l} a$, we obtain the following renormalization group equations:

$$\frac{dK^{-1}}{dl} = \frac{1}{8}y_2^2, \quad \frac{dy_2}{dl} = \left(2 - \frac{K}{2}\right)y_2. \quad (3)$$

These equations show that the y_2 term in eq. (2) is an irrelevant field for $K > 4$ and a relevant field for $K < 4$. On the $K = 4$ line, the BKT transition occurs. Denoting $K = 4 + 2y_1$ near $K = 4$, we have

$$\frac{dy_1(l)}{dl} = -y_2(l)^2, \quad (4)$$

$$\frac{dy_2(l)}{dl} = -y_1(l)y_2(l). \quad (5)$$

The renormalization flow separatrix is given by $y_1(l)^2 - y_2(l)^2 = 0$ ($y_1(l) > 0$). These differential equations are the famous Kosterlitz equations.²¹ On this separatrix, the solution of eqs. (4) and (5) is $y_2(l) = \pm y_1(l) = y_1/(1 + y_1 l)$, where y_1 is the bare coupling constant and $l = 1/\ln L$.

When the y_2 term is relevant, the scaling dimension x should be corrected as $x \rightarrow x + C y_2$. Since the behavior of some scaling dimensions is different depending on whether in the case of relevant y_2 or in the case of irrelevant y_2 , we expect that the BKT transition point can be determined by examining the scaling dimension.

Now, we introduce the dual field $\theta \equiv \theta(\tau, x)$ to the boson field ϕ by the following equations:

$$\partial_\tau \phi = -iK \partial_x \theta, \quad \partial_x \phi = iK \partial_\tau \theta. \quad (6)$$

The vertex operators are expressed in terms of θ and ϕ as

$$V_{n,m} = \exp(in\sqrt{2}\theta) \exp(im\sqrt{2}\phi), \quad (7)$$

where n and m are integers, conventionally called the electric charge and the magnetic charge, respectively. Then, for the free field case ($y_2 = 0$), the scaling dimensions of the vertex operators $V_{n,m}$ are²²

$$x_{n,m} = \frac{1}{2} \left(\frac{n^2}{K} + Km^2 \right). \quad (8)$$

In addition, there is a marginal operator $\mathcal{M} = (\partial_\tau \phi)^2 + (\partial_x \phi)^2$, whose scaling dimension is given by $x_{\text{marg}} = 2$. From the conformal field theory, the eigenvalues $E_{n,m}$ with PBC are related to the scaling dimensions $x_{n,m}$ as²³

$$E_{n,m}(L) - E_g(L) = \frac{2\pi v_s x_{n,m}}{L} \quad (9)$$

in the limit of $L \rightarrow \infty$, where $E_g(L)$ is the ground state energy for the size L system under PBC, and v_s is the spin wave velocity. Using eqs. (8) and (9), we obtain

$$x_{\pm 4,0} = x_{0,\pm 1} = x_{\text{marg}} \quad (10)$$

when $K = 4$ and $y_2 = 0$ (marginal). Considering the invariance under $\phi \leftrightarrow -\phi$, we obtain the combined operators $\cos(\sqrt{2}\phi) \sim V_{0,+1} + V_{0,-1}$ and $\sin(\sqrt{2}\phi) \sim V_{0,+1} - V_{0,-1}$, whose scaling dimensions are $x_{0,\cos}$ and $x_{0,\sin}$, respectively. In the case of $y_2 \neq 0$, these scaling dimensions differ from each other because of the $y_2 \cos(\sqrt{2}\phi)$ term in eq. (2). Thus, $x_{\pm 4,0}$, $x_{0,\cos}$, $x_{0,\sin}$ and x_{marg} are expressed with the logarithmic correction as $x_{\pm 4,0} = 2 - y_1(l)$, $x_{0,\cos} = 2 + 2y_1(l)(1 + 2t/3)$, $x_{0,\sin} = 2 + y_1(l)$ and $x_{\text{marg}} = 2 - y_1(l)(1 + 4t/3)$, where t is a distance from the BKT transition point, defined as $y_2(l) = \pm y_1(l)(1 + t)$. At the BKT transition point ($t = 0$), we have

$$x_{\pm 4,0} = x_{\text{marg}}. \quad (11)$$

Thus we can use this energy level crossing to determine the BKT transition point.¹⁷

Although the above procedure can be applied to determine the BKT transition point, a better method, the twisted-boundary-condition level spectroscopy method, has been proposed.¹⁸ This method is based on the $SU(2)/Z_2$ symmetry on the BKT transition point. We use the following twisted boundary condition (TBC):

$$S_{L+j}^{x,y} = -S_j^{x,y}, S_{L+j}^z = S_j^z. \quad (12)$$

Then, the scaling dimensions of the eigenvalues $E_{n,m}^{\text{TBC}}(L)$ with TBC are given by

$$x_{n,m}^{\text{TBC}} = \frac{1}{2} \left\{ \frac{n^2}{K} + K \left(m + \frac{1}{2} \right)^2 \right\} = x_{n,m+1/2} \quad (13)$$

or

$$E_{n,m}^{\text{TBC}}(L) - E_g(L) = \frac{2\pi v_s}{L} x_{n,m}^{\text{TBC}}. \quad (14)$$

Table I. This table shows relations between quantum numbers (M, P, k) and renormalized scaling dimensions x . $M = \sum_{i=1}^L S_i^z$. BC represents boundary conditions. PBC means periodic boundary condition and TBC means twisted boundary condition. Under TBC, the parity is different from that of PBC, so we use $*$ to classify. $y_2(l) = \pm y_1(l) = y_1/(1 + y_1 l)$, where y_1 is the bare coupling constant and $l = \ln L$.

M	BC	P	k	correction in x	operator in s.G.	scaling dimension
± 2	PBC	1	0	$1/2 - y_1(l)/4$	$\exp(\pm i 2\sqrt{2}\theta)$	$x_{\pm 2,0}$
0	TBC	-1^*		$1/2 + y_1(l)/4 - y_2(l)/2$	$\sin(\phi/\sqrt{2})$	$x_{0,\sin}^{\text{TBC}}$
0	TBC	1^*		$1/2 + y_1(l)/4 + y_2(l)/2$	$\cos(\phi/\sqrt{2})$	$x_{0,\cos}^{\text{TBC}}$

Since we can obtain the half-integer magnetic charge effectively from eq. (13), we now extend the magnetic charge m to that including half-integers. From eqs. (8) and (13), we have in the case of $y_2 = 0$,

$$x_{\pm 2,0} = x_{0,0}^{\text{TBC}} (= x_{0,\pm 1/2}) \quad (15)$$

because $K = 4$. When $y_2 \neq 0$, following the above mentioned way, we define the scaling dimensions $x_{0,\cos}^{\text{TBC}}$ and $x_{0,\sin}^{\text{TBC}}$ of the operators $\cos(\phi/\sqrt{2}) \sim V_{0,+1/2} + V_{0,-1/2}$ and $\sin(\phi/\sqrt{2}) \sim V_{0,+1/2} - V_{0,-1/2}$, respectively, and also we express these scaling dimensions with the logarithmic correction as shown in Table I. At the BKT transition point ($y_2 = \pm y_1$, $y_1 > 0$), we have

$$x_{\pm 2,0} = x_{0,\sin}^{\text{TBC}}. \quad (16)$$

Since the electric charge and the magnetic charge of $x_{\pm 2,0}$ and $x_{0,\sin}^{\text{TBC}}$ are smaller than those of $x_{\pm 4,0}$ and x_{marg} , we can obtain more accurate results by using the twisted-boundary-condition level spectroscopy method¹⁸ than those by using the original level spectroscopy method.¹⁷

We can identify the correspondence between the operators in the boson representation and the eigenstates of spin chains by comparing their symmetry properties¹⁸ as shown in Table I. The Hamiltonian of eq. (1) with PBC is invariant under the spin rotation around the z-axis, the translation ($\mathbf{S}_i \rightarrow \mathbf{S}_{i+1}$) and the space inversion ($\mathbf{S}_i \rightarrow \mathbf{S}_{N-i+1}$). The quantum numbers corresponding to these invariance are $M \equiv \sum_{i=1}^L S_i^z$, $k = 2\pi n/L$ ($n = 0, \dots, L/2 - 1$) and $P = \pm 1$, respectively. From Table I, we see that $x_{\pm 2,0}$ corresponds to the lowest excitation energy with $M = \pm 2$, $P = 1$, $k = 0$, and $x_{0,\sin}^{\text{TBC}}$ to the lowest excitation energy with $M = 0$, $P = -1^*$ under TBC. The energy level crossing of these two energies for $L = 16$ and $\Delta = -0.2$ is shown in Fig. 2.

In addition to the logarithmic correction, there is another correction between a lattice system and a continuous model. Considering the $x = 4$ irrelevant field operator $L_{-2}\bar{L}_{-2}\mathbf{1}$

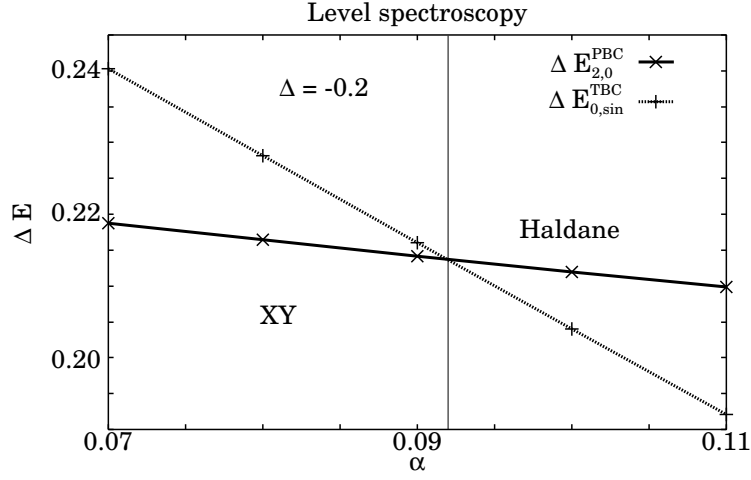


Fig. 2. Energy level crossing between $x_{2,0}$ and $x_{0,\sin}^{\text{TBC}}$ when $L = 16$ and $\Delta = -0.2$. The value of α_c^{BKT} is obtained to be $\alpha_c^{\text{BKT}} = 0.09193$.

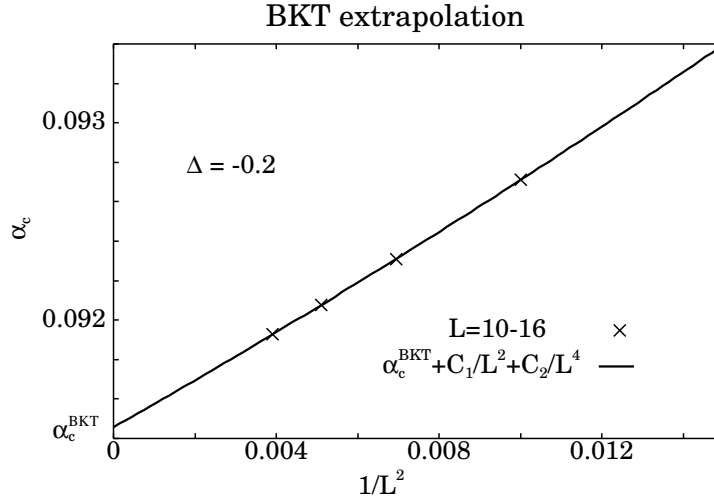


Fig. 3. Extrapolation procedure of α_c^{BKT} for $\Delta = -0.2$, where a fitting function $\alpha(L) = \alpha_c^{\text{BKT}} + C_1/L^2 + C_2/L^4$, is assumed.

in terms of the conformal field theory,²⁴ we should extrapolate the infinite-size critical point α_c^{BKT} as

$$\alpha(L) = \alpha_c^{\text{BKT}} + C_1/L^2 + C_2/L^4. \quad (17)$$

The BKT transition point for $\Delta = -0.2$ is determined as shown in Fig. 3. The same procedure can be carried out varying α with fixed Δ , and the obtained BKT transition line is represented in Fig. 1.

Next, in order to check the consistency of the universality class, we confirm that two universal relations, concerning the central charge c and the energy gap ratio, hold in the

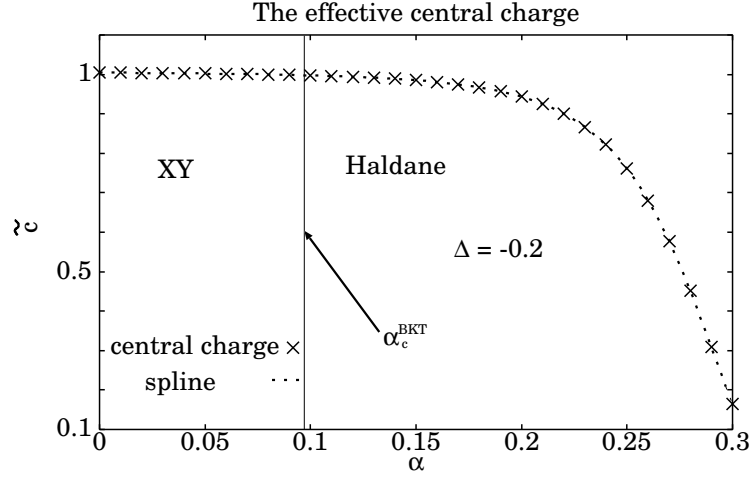


Fig. 4. Plot of the effective central charge \tilde{c} as a function of α for $\Delta = -0.2$. In the massless region, $\tilde{c} = 1$. The BKT transition occurs at α_c^{BKT} .

following way.

The BKT transition line is expected to be described by the conformal field theory with the central charge $c = 1$. It is well known that the finite-size correction to the ground state energy is related to the central charge c and the spin wave velocity v_s as follows,^{23–26}

$$\frac{1}{L}E_g(L) \cong \varepsilon_\infty - \frac{\pi c v_s}{6L^2}, \quad (18)$$

where

$$v_s = \lim_{L \rightarrow \infty} \frac{L}{2\pi} \{E_{k_1}(L) - E_g(L)\}. \quad (19)$$

Here $E_{k_1}(L)$ is the energy of the excited state with wave number $k_1 = \frac{2\pi}{L}$ and magnetization $M = 0$. In general, we should obtain v_s as

$$v(L) = v_s + C_1/L^2 + C_2/L^4. \quad (20)$$

Although there remain logarithmic corrections in the central charge, which is obtained from eq. (18), they are small enough to be $O(1/(\ln L)^3)$.²⁷ Thus we neglect them. It is proper that the effective central charge \tilde{c} should correspond to the central charge c in a massless region. In a massive region, the correction term in eq. (18) is modified as $1/L^2 \rightarrow \exp(-L/\xi)$. We calculate the effective central charge \tilde{c} , the result of which is shown in Fig. 4. We can see that the effective central charge changes rapidly from $\tilde{c} = 1$ (massless) to $\tilde{c} = 0$ (massive). This fact agrees with previous results in refs. 28 and 29.

Next, we examine the ratio of the energy levels. From eqs. (8) and (9), we obtain

$$\frac{\Delta E_2}{\Delta E_1} = 4, \quad (21)$$

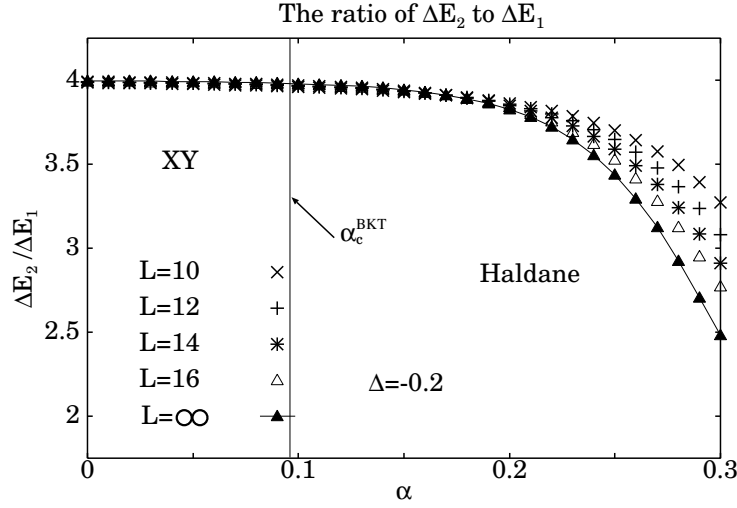


Fig. 5. Plot of $\Delta E_2/\Delta E_1$ as a function of α for $\Delta = -0.2$. In the XY phase, $\Delta E_2/\Delta E_1 = 4$, and in the gapful phase, $\Delta E_2/\Delta E_1 = 2$. Because of the finite-size effect, $\Delta E_2/\Delta E_1$ varies slowly.

where $\Delta E_i = E(M = \pm i) - E_g(M = 0)$ ($i = 1, 2$). This relation is independent of K . In the gapful (massive) phase, on the other hand, we have

$$\frac{\Delta E_2}{\Delta E_1} \rightarrow 2 \quad (L \rightarrow \infty), \quad (22)$$

since the mass of two magnons is twice as large as that of one magnon when each magnons are independent. This ratio varying with α in the case of $\Delta = -0.2$ is shown in Fig. 5. We can also see the size dependence of $\Delta E_2/\Delta E_1$. Affected by the $x = 4$ irrelevant field operator $L_{-2}\bar{L}_{-2}\mathbf{1}$, the extrapolated value, described in Fig. 5, can be given as follows,

$$\mathcal{O} = \mathcal{O}_\infty + C_1/L^2 + C_2/L^4, \quad (23)$$

where \mathcal{O} means $\Delta E_2/\Delta E_1$. It appears that the ratio is 4 in the massless phase and it changes very slowly from 4 to 2 because of the finite-size effect.

3.2 Instability of ferromagnetic phase

We determine the unstable boundary of the ferromagnetic phase as follows. If there is no intermediate phase, we can obtain the boundary of the ferromagnetic phase by examining the energy level crossing between the energy of the ferromagnetic state, $E = (1 + \alpha)\Delta L$, and that of the $M = 0$ state. Moreover, we compare the numerical result with that obtained by the ferromagnetic spin wave theory (see APPENDIX A).

The phase diagram near the ferromagnetic phase determined by these two methods is shown in Fig. 6. Below $\alpha = 0.38$, the ferromagnetic stable line obtained from the diagonalization data agrees with the line determined by the spin wave theory. The fact that the convergence of the ferromagnetic boundary depending on L is not so good above $\alpha = 0.38$ suggests that the incommensurability begins to modulate the ground state energy. The be-

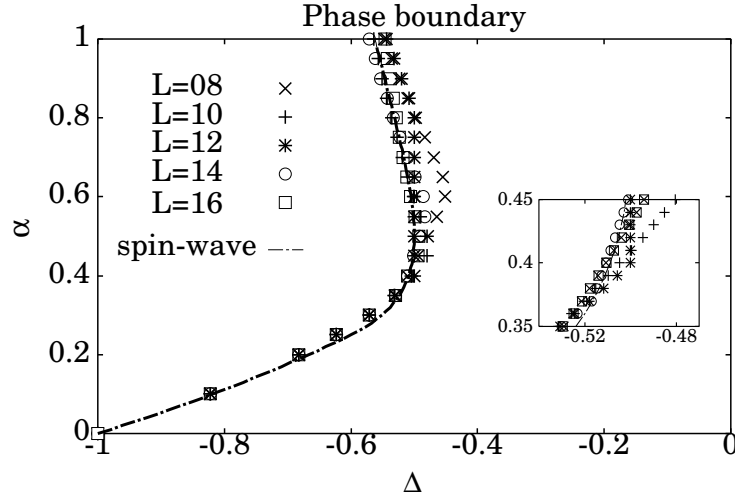


Fig. 6. Phase boundary of the ferromagnetic phase, obtained by the energy level crossing from the diagonalization data and the spin wave theory.

havior of the ferromagnetic phase boundary obtained by the energy level crossing is, however, analogous to that by the spin wave theory. Therefore, we adopt the line of the spin wave theory as the ferromagnetic phase boundary in Fig. 1.

3.3 Haldane-Néel transition

The phase transition between the Haldane phase and the Néel phase belongs to the second order phase transition. In order to determine the transition line between these phases, we apply the PRG method.^{19,20} This method is explained as follows. In the Néel phase, the ground state is twofold degenerate in the thermodynamic limit. For finite L , however, this degeneracy is splitting into two energy levels. The energy gap between these energy levels is $\Delta E(L, \alpha, \Delta) = E(M = 0, P = -1, k = \pi) - E_g(M = 0, P = 1, k = 0)$, which behaves as $\Delta E \sim \exp(-L/\xi)$ in the $L \rightarrow \infty$ limit. On the other hand, the Haldane state has the energy gap, which remains finite in the thermodynamic limit. Thus the product $L\Delta E(L)$ increases (decreases) with L for $\Delta < \Delta_c^{\text{HN}}$ ($\Delta > \Delta_c^{\text{HN}}$), where Δ_c^{HN} means the critical value of Δ at the Haldane-Néel transition. Therefore, we use the following equation to determine the Haldane-Néel transition:

$$L\Delta E(L, \alpha, \Delta_c(L, L+2)) = (L+2)\Delta E(L+2, \alpha, \Delta_c(L, L+2)). \quad (24)$$

The Δ -dependences of $L\Delta E(L)$ with $\alpha = -0.5$ for various L are shown in Fig. 7. We extrapolate the infinite-size critical point Δ_c^{HN} as follows:

$$\Delta_c(L, L+2) = \Delta_c^{\text{HN}} + \frac{C_1}{(L+1)^2} + \frac{C_2}{(L+1)^4}. \quad (25)$$

When $\alpha = -0.5$, the infinite-size transition point Δ_c^{HN} is determined as shown in Fig. 8. The same procedure can be carried out by varying Δ with fixed α . The obtained Haldane-Néel transition line is shown in Fig. 1 and also in Fig. 9 together with the finite-size results.

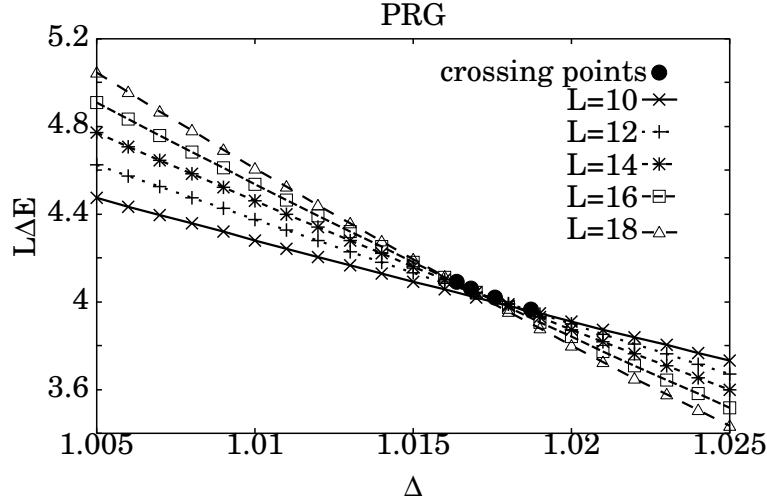


Fig. 7. The Δ dependence of $L\Delta E(L)$ with $\alpha = -0.5$ for $L = 10, 12, 14, 16$ and 18 . The crossing points (\bullet) are the finite-size transition points.

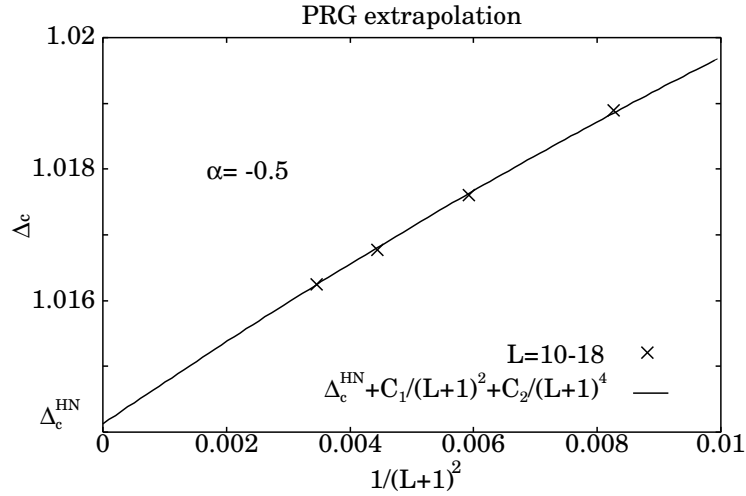


Fig. 8. Extrapolation procedure of Δ_c^{HN} for $\alpha = -0.5$, where a fitting function $\Delta_c(L, L+2) = \Delta_c^{\text{HN}} + C_1/(L+1)^2 + C_2/(L+1)^4$ is assumed.

From the quantum Monte Carlo simulation in the case of $\alpha = 0$,¹³ this transition has been known to belong to the 2D-Ising type universality class. Therefore, we expect that the universality class of the whole Haldane-Néel transition line is of the 2D-Ising type.

4. The analysis of the anisotropic non-linear σ model

In order to examine whether the Haldane phase does or does not survive in the region of $\alpha \ll -1$ and $\Delta \sim 1$, we perform the following analytical calculation, the details of which is discussed in APPENDIX B. First, we map the spin- s (s is integer) XXZ spin chain with NNN

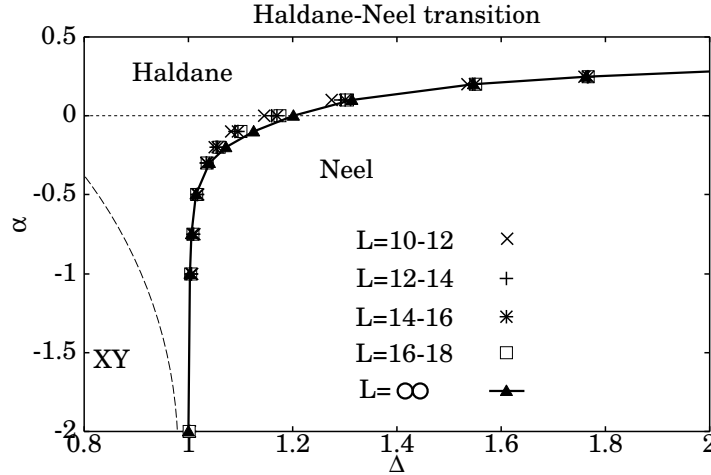


Fig. 9. Phase diagram near the Haldane-Néel transition line.

interaction onto the non-linear σ model with Ising-type anisotropy Δ in the large- s limit.^{30–32} Then, we obtain the renormalization group equation (eq. (B-19)) from the non-linear σ model by using the renormalization group method.³³ From this equation, the renormalization group flows are represented by Δ and α as

$$|\Delta - 1| \propto \frac{\sqrt{1 - 4\alpha}}{1 - \alpha} \exp(-2\pi\sqrt{1 - 4\alpha}), \quad \text{when } |\Delta - 1| \ll 1. \quad (26)$$

We assume that these renormalization group flows are connected to each renormalization group fixed point: the XY or the Ising fixed point. These fixed points may be asymmetric on the phase diagram. Therefore, we can draw the schematic phase diagram, comparing with the numerical data, as shown in Fig. 10. The numerical results are in good agreement with the analytical lines near $\Delta \sim 1$ and $\alpha \sim -1$.

The phase is massive at the isotropic point, $\Delta = 1$ and $\alpha \rightarrow -\infty$, since the mass term (eq. (B-20)) exists. Thus, we may conclude that the phase transition between the XY phase and the Néel phase does not directly occur in this limit and the Haldane phase appears between these two phases.

5. SUMMARY AND DISCUSSION

The ground state phase diagram of the $S = 1$ XXZ chain with NNN interaction has been determined numerically by analyzing the numerical diagonalization data using the twisted-boundary-condition level spectroscopy method¹⁸ and the phenomenological renormalization group method,^{19,20} and analytically by the spin wave theory. Particularly, it has been resolved that the phase transition between the XY phase and the Néel phase does not occur directly for $\alpha \ll -1$ near $\Delta = 1$ by mapping onto the non-linear σ model^{30–32} and using the renormalization group method.³³

In this paper, we have not treated the region for $\alpha > 0.4$, except for the vicinity of the

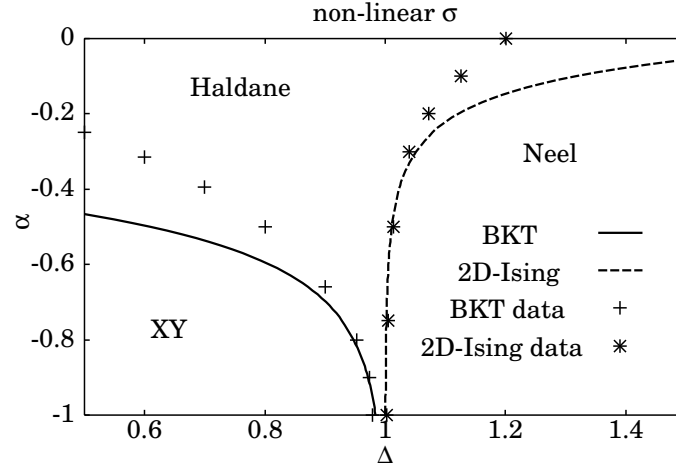


Fig. 10. Phase diagram near the $\alpha = -1$ and $\Delta = 1$ point. We compare the schematic phase diagram obtained from eq. (26) with the numerically extrapolated data to $L \rightarrow \infty$. The numerical results are in good agreement with the analytical line near $\Delta = 1$ and $\alpha = -1$.

ferromagnetic phase, because of the incommensurability. When $\Delta = 1.0$, the commensurate-incommensurate (C-IC) change is known to occur at $\alpha = \alpha_{\text{C-IC}}$, where $\alpha_{\text{C-IC}} \sim 0.28$ is obtained by the DMRG method^{8,9} and $\alpha_{\text{C-IC}} \sim 0.38$ by the diagonalization technique.³⁴ Note that this C-IC change is not a phase transition because the energy gap does not vanish.

In principle, the phase transition line between the Haldane phase and the double Haldane phase can be determined by Kitazawa's twisted-boundary-condition level spectroscopy method.³⁵ However, we failed to determine this transition line by this method. Since the ground state energy is modulated with the long wave length in the incommensurate region, the extrapolation procedure is difficult. In this region, some long range orders, chiral order and string order, exist, and therefore the infinite-system DMRG method is known to be relatively useful.^{6,7} However, it is difficult to determine phase boundaries of the gapless chiral phase, where the string order parameter is exhibiting a quasi-long-range order, by using the DMRG method. In order to advance the analysis of the incommensurate region, we need to investigate the incommensurability and we must find an effective method to treat this nasty problem.

Acknowledgments

The numerical calculation in this work is based on the program packages TITPACK version 2, developed by Professor H. Nishimori, and KOBEPACK/S, coded by Professor M. Kaburagi. This work is partly supported by a Grant-in-Aid for Scientific Research on Priority Areas (B) ('Field-Induced New Quantum Phenomena in Magnetic Systems') from the Ministry of Education, Culture, Sports, Science and Technology of Japan. We further thank the Supercomputer Center, Institute for Solid State Physics, University of Tokyo, the Infor-

mation Synergy Center, Tohoku University, and the Computer Room, Yukawa Institute for Theoretical Physics, Kyoto University for computational facilities.

Appendix A: The analysis of spin wave instability

In this Appendix, we consider the instability analysis of the ferromagnetic phase of the spin- s XXZ chain with NNN interaction. We consider the Hamiltonian of eq. (1), but S^x, S^y and S^z are spin- s operators now. When we denote the fully ferromagnetic state by $|0\rangle$, we obtain the ground state energy for the fully ferromagnetic phase as

$$\mathcal{H}|0\rangle = E_0|0\rangle, \quad (\text{A}\cdot 1)$$

where $E_0 = \Delta s^2 L + \alpha \Delta s^2 L$ and s is the eigen value of S^z for $|0\rangle$. Then, in order to see the lowest excitation, we consider the following operator which is the linear combination of the spin lowering operator,

$$\sum_m S_m^- \exp(-ikm), \quad (\text{A}\cdot 2)$$

where k is the wave number. When this operator acts on $|0\rangle$, we obtain

$$\mathcal{H} \sum_m S_m^- \exp(-ikm)|0\rangle = \{E_0 + \omega(k)\} \sum_m S_m^- \exp(-ikm)|0\rangle, \quad (\text{A}\cdot 3)$$

where $\omega(k)$ represents the dispersion relation,

$$\omega(k) = 2s\{(\cos k - \Delta) + \alpha(\cos 2k - \Delta)\} \quad (\text{A}\cdot 4)$$

$$= 2s \left\{ 2\alpha \left(\cos k + \frac{1}{4\alpha} \right)^2 - \frac{1}{8\alpha} - \alpha - \Delta - \alpha\Delta \right\}. \quad (\text{A}\cdot 5)$$

If $\omega(k)$ is negative, the fully ferromagnetic state is unstable because of the spin wave excitation. Therefore we can regard the line of $\omega(k) = 0$ as the ferromagnetic stable-unstable boundary. Since the prefactor $2s$ is positive, we omit $2s$ in the following analysis.

From eq. (A-5), we can see that the minimum value of the dispersion $|\omega(k)|$ is different whether in the case of $\alpha > 1/4$ or in the case of $\alpha \leq 1/4$. In order to examine the incommensurate region, it is enough to consider for $\alpha > 0$.

In the former case, $|\omega(k)|$ has a minimum value when $k = \pm \arccos \frac{-1}{4\alpha}$. Then, we have

$$\Delta = -\frac{1 + 8\alpha^2}{8\alpha(1 + \alpha)}. \quad (\text{A}\cdot 6)$$

Therefore the fully ferromagnetic phase becomes unstable for $k = \pm \arccos \frac{-1}{4\alpha}$ modes of the spin wave excitation. Classically, these modes are connected with incommensurability.

In the latter case, $|\omega(k)|$ is minimum when $k = \pm\pi$. Then, we have

$$\Delta = \frac{\alpha - 1}{\alpha + 1}. \quad (\text{A}\cdot 7)$$

Therefore the fully ferromagnetic phase becomes unstable for $k = \pm\pi$ mode of the spin wave excitation.

Appendix B: The non-linear σ model

The spin- s XXZ chain can be mapped onto the non-linear σ model with Ising-type anisotropy in the large- s limit.^{30–32}

We first consider the antiferromagnetic Heisenberg Hamiltonian with NNN interaction α :

$$\mathcal{H} = \sum_i \mathbf{S}_i \cdot \mathbf{S}_{i+1} + \alpha \sum_i \mathbf{S}_i \cdot \mathbf{S}_{i+2} \quad (\text{B.1})$$

with $\alpha < 0$. We want to keep low energy modes as follows,

$$\mathbf{S}_i \simeq (-1)^i s \boldsymbol{\varphi}_i + a \mathbf{l}_i, \quad (\text{B.2})$$

where $\boldsymbol{\varphi}$ corresponds to the Fourier mode with the wave number $k \simeq \pi$, and \mathbf{l} corresponds to the Fourier mode with the wave number $k \simeq 0$. These operators are defined as

$$\boldsymbol{\varphi} \left(2i + \frac{1}{2} \right) = \frac{(\mathbf{S}_{2i+1} - \mathbf{S}_{2i})}{2s}, \quad (\text{B.3})$$

$$\mathbf{l} \left(2i + \frac{1}{2} \right) = \frac{(\mathbf{S}_{2i+1} + \mathbf{S}_{2i})}{2a}. \quad (\text{B.4})$$

where a is the lattice spacing. Note that $\boldsymbol{\varphi}$ and \mathbf{l} are slowly varying function of i . In the continuous limit, these operators obey the following commutators,

$$[l^\alpha(x), l^\beta(y)] = i\varepsilon^{\alpha\beta\gamma} l^\gamma(x) \delta(x-y), \quad (\text{B.5})$$

$$[l^\alpha(x), \varphi^\beta(y)] = i\varepsilon^{\alpha\beta\gamma} \varphi^\gamma(x) \delta(x-y), \quad (\text{B.6})$$

$$[\varphi^\alpha(x), \varphi^\beta(y)] = i\varepsilon^{\alpha\beta\gamma} l^\gamma(x) \delta(x-y) 2a \frac{1}{4s^2} \rightarrow 0, \quad (\text{B.7})$$

where $\{\alpha, \beta, \gamma\} = \{x, y, z\}$ and $\varepsilon^{\alpha\beta\gamma}$ is the three-dimensional Levi-Civita symbol. Repeated indices are normally summed. These operators satisfy the following constraints,

$$\boldsymbol{\varphi} \cdot \mathbf{l} = 0, \quad (\text{B.8})$$

$$|\boldsymbol{\varphi}|^2 = 1. \quad (\text{B.9})$$

Now, the Hamiltonian density can be mapped onto the $O(3)$ non-linear σ model,

$$\mathcal{H} = \frac{v}{2} \left\{ g \left(1 - \frac{\theta}{4\pi} \frac{\partial \boldsymbol{\varphi}}{\partial x} \right)^2 + \frac{1}{g} \left(\frac{\partial \boldsymbol{\varphi}}{\partial x} \right)^2 \right\}, \quad (\text{B.10})$$

where the velocity $v = 2sa$, the topological angle $\theta = 2\pi s$ and the coupling constant $g = \frac{2}{s\sqrt{1-4\alpha}}$.

Next, we consider the Hamiltonian with Ising-type anisotropy Δ as follows,

$$\mathcal{H} = \sum_i \mathbf{S}_i \cdot \mathbf{S}_{i+1} + \alpha \sum_i \mathbf{S}_i \cdot \mathbf{S}_{i+2} + \sum_i \{ (\Delta - 1) S_i^z S_{i+1}^z + \alpha (\Delta - 1) S_i^z S_{i+2}^z \}. \quad (\text{B.11})$$

We only choose the leading term in the anisotropic terms as

$$S_i^z S_{i+1}^z \sim -s^2 \varphi_z^2, \quad (\text{B.12})$$

$$S_i^z S_{i+2}^z \sim s^2 \varphi_z^2. \quad (\text{B.13})$$

Then, we obtain the following effective Hamiltonian density,

$$\mathcal{H} = \frac{v}{2} \left\{ g \left(1 - \frac{\theta}{4\pi} \frac{\partial \varphi}{\partial x} \right)^2 + \frac{1}{g} \left(\frac{\partial \varphi}{\partial x} \right)^2 \right\} + \frac{vm^2}{2g} \varphi_z^2, \quad (\text{B}\cdot 14)$$

where

$$m^2 = \frac{2(\Delta - 1)(-1 + \alpha)}{a^2(1 - 4\alpha)^{1/2}}. \quad (\text{B}\cdot 15)$$

We have obtained the Hamiltonian density of the anisotropic non-linear σ model. The corresponding Euclidean (2-D classical) Lagrangian density is^{30–32}

$$\mathcal{L} = \frac{1}{2g} \left\{ (\partial_\mu \varphi)^2 + m^2 \varphi_z^2 + \frac{\theta}{8\pi} \epsilon^{\mu\nu} \varphi \cdot (\partial_\mu \varphi \times \partial_\nu \varphi) \right\} \quad (\text{B}\cdot 16)$$

where we set $v = 1$ for this discussion. Since we take an integer spin case, we can neglect the topological term.

Renormalization group equations of this model without the topological term are obtained by Nelson and Pelcovits.³³ Since $d = 2$ (dimension) and $n = 3$ (number of components) in our case, we obtain the differential equations for the “dressed” coupling constant \tilde{g} and the “dressed” mass \tilde{m} :

$$\frac{d\tilde{g}}{d \ln b} = \frac{1}{2\pi} \left(\frac{\tilde{g}^2}{1 + \tilde{m}^2} \right), \quad (\text{B}\cdot 17)$$

$$\frac{d\tilde{m}^2}{d \ln b} = 2\tilde{m}^2 - \frac{1}{\pi} \frac{\tilde{g}\tilde{m}^2}{1 + \tilde{m}^2}. \quad (\text{B}\cdot 18)$$

Removing $\ln b$, we can obtain the renormalization relation between \tilde{m}^2 and \tilde{g} ,

$$\frac{d\tilde{m}^2}{d\tilde{g}} = \frac{4\pi}{\tilde{g}^2} \tilde{m}^2 (1 + \tilde{m}^2) - \frac{2\tilde{m}^2}{\tilde{g}}. \quad (\text{B}\cdot 19)$$

Therefore, the relation between the dressed \tilde{m}^2 and the dressed \tilde{g} is

$$\tilde{m}^2(\tilde{g}) \propto \exp \left(-\frac{4\pi}{\tilde{g}} \right). \quad (\text{B}\cdot 20)$$

For $\tilde{m}^2 > 0$, all flow lines terminate in a fixed line at $\tilde{m}^2 = +\infty$. One of these lines is believed to terminate at the BKT transition point \tilde{g}_c . Therefore, this flow line should be a critical line between the XY phase and the disordered (Haldane) phase. From the similar discussion, we obtain the Ising critical line for $\tilde{m}^2 < 0$ case. Finally, in terms of the original Hamiltonian (eq. (B·11)) by the use of eq. (B·15), we now obtain the critical line eq.(26) expressed as

$$|\Delta - 1| \propto \frac{\sqrt{1 - 4\alpha}}{1 - \alpha} \exp(-2\pi\sqrt{1 - 4\alpha}). \quad (\text{B}\cdot 21)$$

Note that eq. (B·21), or eq. (26), can be extended to the $\alpha \rightarrow -\infty$ limit.

References

- 1) F. D. M. Haldane: Phys. Lett. **93A** (1983) 464.
- 2) F. D. M. Haldane: Phys. Rev. Lett. **50** (1983) 1153.
- 3) H. Kikuchi, M. Chiba and T. Kubo: Can. J. Phys. **79** (2001) 1551.
- 4) T. Masuda, T. Sakaguchi and K. Uchinokura: J. Phys. Soc. Jpn. **71** (2002) 2637.
- 5) T. Tonegawa, S. Suzuki and M. Kaburagi: J. Magn. Magn. Mater. **140-144** (1995) 1613.
- 6) M. Kaburagi, H. Kawamura and T. Hikihara: J. Phys. Soc. Jpn. **68** (1999) 3185.
- 7) T. Hikihara, M. Kaburagi, H. Kawamura and T. Tonegawa: J. Phys. Soc. Jpn. **69** (2000) 259.
- 8) A. Kolezhuk, R. Roth and U. Schollwöck: Phys. Rev. Lett. **25** (1996) 5142.
- 9) A. Kolezhuk, R. Roth and U. Schollwöck: Phys. Rev. B **55** (1997) 8928.
- 10) A. Kitazawa, K. Nomura and K. Okamoto: Phys. Rev. Lett. **76** (1996) 4038.
- 11) A. Kitazawa and K. Nomura: J. Phys. Soc. Jpn. **66** (1997) 3944.
- 12) W. Chen, K. Hida and B. C. Sanctuary: Phys. Rev. B **67** (2003) 104401.
- 13) K. Nomura: Phys. Rev. B **40** (1989) 9142.
- 14) H. J. Schulz: Phys. Rev. B **34** (1986) 6372.
- 15) P. Lecheminant, T. Jolicoeur and P. Azaria: Phys. Rev. B **63** (2001) 174426.
- 16) A. Kitazawa, K. Hijii and K. Nomura: J. Phys. A **36** (2003) L351.
- 17) K. Nomura: J. Phys. A **28** (1995) 5451.
- 18) K. Nomura and A. Kitazawa: J. Phys. A **31** (1998) 7341.
- 19) M. N. Barber: Phase transition and Critical Phenomena, ed. C. Domb and J. L. Lebowitz (ACADEMIC PRESS, 1983) Vol. 8, p. 145.
- 20) H. H. Roomany and H. W. Wyld: Phys. Rev. D **21** (1980) 3341.
- 21) J. M. Kosterlitz: J. Phys. C **7** (1974) 1046.
- 22) L. P. Kadanoff and A. C. Brown: Ann. Phys. **121** (1979) 318.
- 23) J. L. Cardy: J. Phys. A **17** (1984) L385.
- 24) J. L. Cardy: Nucl. Phys. B **270**[FS16] (1986) 186.
- 25) H. W. Blöte, J. L. Cardy and M. P. Nightingale: Phys. Rev. Lett. **56** (1986) 742.
- 26) I. Affleck: Phys. Rev. Lett. **56** (1986) 746.
- 27) J. L. Cardy: J. Phys. A **19** (1986) L1093; J. Phys. A **20** (1987) 5039(E)
- 28) H. Inoue and K. Nomura: Phys. Lett. A **262** (1999) 96.
- 29) H. Inoue: Phys. Lett. A **270** (2000) 359.
- 30) I. Affleck: Phys. Rev. Lett. **56** (1986) 408.
- 31) I. Affleck: J. Phys. Cond. Matt. **1** (1989) 3047.
- 32) I. Affleck: Fields, Strings and Critical Phenomena Les Houches XLIX 1988, ed. E. Brezin and J. Zinn-Justin (Amsterdam: North-Holland, 1990) p. 563.
- 33) D. R. Nelson and R. A. Pelcovits: Phys. Rev. B **16** (1977) 2191.
- 34) T. Tonegawa, M. Kaburagi, N. Ichikawa and I. Harada: J. Phys. Soc. Jpn. **61** (1992) 2890.
- 35) A. Kitazawa: J. Phys. Soc. Jpn. **30** (1997) L285.